HAL
archives-ouvertes.fr

Behaviour of a double layer tensegrity grid under static loading: identification of self-stress level

Nicolas Angellier, Jean-François Dubé, Jérôme Quirant, Bernard Crosnier

▶ To cite this version:

HAL Id: hal-00858716
https://hal.archives-ouvertes.fr/hal-00858716

Submitted on 18 Oct 2016

Behavior of a Double-Layer Tensegrity Grid under Static Loading: Identification of Self-Stress Level

Nicolas Angellier[1]; Jean François Dubé[2]; Jérôme Quirant[3]; and Bernard Crosnier[4]

Abstract: The determination of the state of internal stress is important to define the rigidity of a tensegrity structure and its stability. Several methods can be used; some are based on direct measurements of the forces in the elements, but are not easily transferable to a real structure. The authors opt for indirect measurement techniques, which seem more appropriate for implementation on-site. One can consider the vibratory anal-ysis of the elements, the vibratory analysis of the whole structure, or the analysis of the structure's behavior under static loading. Here, the node displacement fields of a tensegrity structure in different states of self-stress under several strategies of static loadings is studied by comparing the measurement obtained by a tachometer with simulations. The aim of this work is to show the feasibility of a displacement field to identify the state of self-stress by this analysis. It is shown that under certain conditions, plans can be made to replace the direct measurement of the forces by indirect analysis.

Keywords: Tensegrity; Tachometer; Self-stress; Field measurement; Inverse analysis.

Introduction

Tensegrity systems constitute a particular class of space structures. They are autonomous lattice systems stabilized by an initial self-stress state (Motro 2003). Inspiring architects, they make it possible to conceive light and visually transparent structures (Snelson 1973; Fuller 1973). Despite their advantages, real projects based on tensegrity principles are still rare. Indeed, the few existing achievements are not well documented regarding the crucial steps of adjustment of the initial self-stress state (Averseng and Crosnier 2004a; Kawaguchi and Lu 2002; Oda and Hangai 1995). There is no code of practice available for this type of construction. In addition, these systems still have to prove their advantages when compared with traditional lattice systems. Tensegrity grids are composed of compressed struts and tensioned cables. Struts are generally subjected to weak stress compared with yield strength. The cables, on the other hand, are the most sensitive elements of the system. They ensure its stability and stiffness: pretensioning generates tension stress, which can be close to the yield stress. Previous theoretical and numerical studies are developed and compared on real tensegrity grids, designed during the Tensarch project (Motro 2002). For example, original methods have been developed for self-stress control (identi-fication of the internal state and determination of length corrections of elements to achieve a target state through numerical simulation) and the active control of behavior (Averseng and Crosnier 2004b). It is nec-essary to determine the evolution of cable tension during the lifetime of a structure. There are several sources of that variation. Some, such as the clearance adjustment of connections or strand rearrangements, produce a fast evolution when the structure is assembled. Others, such as creep, relieving, and slipping connectors, produce a slow evolution of ten-sions. Finally, external, mechanical, or thermal loadings can also generate variations in cable tension. It is not conceivable to analyze the tension of each cable locally, because each cable should be equipped with a specific sensor. Among the measurements that can be carried out easily, those related to displacement fields and eigenfrequencies of the structure are widely used (Van Den Abeele and DeVisscher 2000; Maeck et al. 2000; Murakami and Nishimura 2001; Ndambi 2000; Pritchard et al. 1987). The damage acting in an element and its lo-calization is obtained by inverse analysis (Barcilon 1982; Bicanic and Chen 1997; Dubé 2004). The method is the same as the one used for structure optimization (Olhof et al. 1997; Gurdal et al. 1993). The direct measurement of the forces in the elements showed the weaknesses of indirect measurements previously used to evaluate the self-stress state (Dubé et al. 2008). For further studies on these grids, the authors tooled up a precision tachometer that measures the node positions with an estimated accuracy of less than 0.2 mm. This enables the displacement fields of the whole structure's nodes to be surveyed, subjected to a static loading. A numerical study evaluated the sensitivity of these dis-placement fields to the self-stress level (Angellier et al. 2009). Here, a complete experimental study using the tachometric measuring device succeeds in estimating the accuracy of self-stress level identification.

Tensegrity Grid

Minigrid

This minigrid is the prototype of the Tensarch project's grid (Motro 2002). It is a double-layer plane grid of cables, the basic

[1]Associate Professor, Université de Limoges, Groupe d'Etudes des Matériaux Hétérogènes, Génie Civil & Durabilité, 19300 Egletons, France (corresponding author). E-mail: nicolas.angellier@unilim.fr

[2]Professor, Laboratoire de Mécanique et Génie Civil-Unité Mixte de Recherche 5508, F-34095 Montpellier Cedex 5, France. E-mail: dube@lmgc.univ-montp2.fr

[3]Associate Professor, Laboratoire de Mécanique et Génie Civil-Unité Mixte de Recherche 5508, F-34095 Montpellier Cedex 5, France. E-mail: quirant@lmgc.univ-montp2.fr

[4]Professor, Laboratoire de Mécanique et Génie Civil-Unité Mixte de Recherche 5508, F-34095 Montpellier Cedex 5, France. E-mail: crosnier@lmgc.univ-montp2.fr

pattern of which uses the expander principle: 2×2, the struts form perpendicular, opposing Vs, separated by a vertical tie the length of which can be made to vary. This consists of 81 components linked by nodes: 24 compressed struts (steel tubes) and tensioned elements, that is, 36 cables (single-strand stainless steel) in addition to nine vertical ties and 12 peripheral ties (hot drawn steel); the ties are the active components of the structure (Fig. 1). This grid has been designed to match the definition of a tensegrity structure: "system in a state of self-stable equilibrium (self-stress here), which includes a discontinuous set of compressed components (bars) inside a continuum of tensioned components (cables and ties)" (Motro 2003).

Self-Stress State

The system equilibrium is obtained when all nodes are in equilibrium (Fig. 2). The static equilibrium of node i is written as in Fig. 2.

N_{ij} is the internal force vector of the element linking node j to node i, and F_i is the external force vector directly applied to node i. The internal forces T_{ij} are a function of the deformation of each element; x_i, y_i, and z_i are spatial coordinates of node i, and L_{ij}, the length of the element connecting nodes i and j in the reference

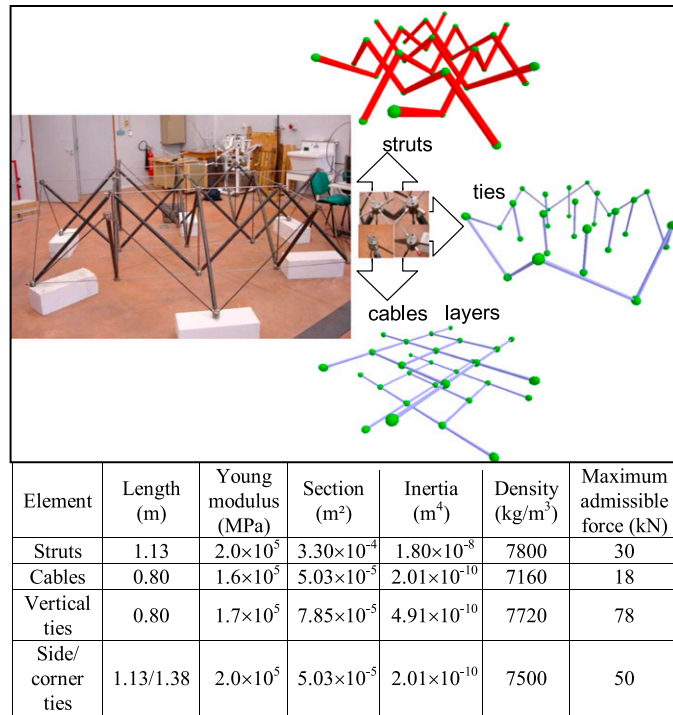| Element	Length (m)	Young modulus (MPa)	Section (m²)	Inertia (m⁴)	Density (kg/m³)	Maximum admissible force (kN)
Struts	1.13	2.0×10^5	3.30×10^{-4}	1.80×10^{-8}	7800	30
Cables	0.80	1.6×10^5	5.03×10^{-5}	2.01×10^{-10}	7160	18
Vertical ties	0.80	1.7×10^5	7.85×10^{-5}	4.91×10^{-10}	7720	78
Side/ corner ties	1.13/1.38	2.0×10^5	5.03×10^{-5}	2.01×10^{-10}	7500	50

Fig. 1. Minigrid, elements characteristics, and modeling

configuration. The projection of the equilibrium equation can be simplified by introducing force density q_{ij} of each element (i, j). The system of equations obtained by applying equations to all the nodes of the structure is

$$\mathbf{Aq} = \mathbf{f} \quad (1)$$

where $\mathbf{A}$ = equilibrium matrix of the structure (dimension $b \times 3n$), $\mathbf{q}$ = vector describing the force densities in elements b, and $\mathbf{f}$ = vector of the external forces acting on nodes n. The self-stress state verifies the global static equilibrium of the system under no external load. Therefore, it is the solution to the problem [Eq. (1)] with $\mathbf{f} = 0$, which is by definition the kernel of equilibrium matrix $\mathbf{A}$. The subspace $ker\mathbf{A}$ is a base, denoted by S, composed of several basic self-stress states. Because the behavior of a tensegrity system is subject to several sources of nonlinearity, mainly because of the unilateral behavior of cables and second-order transverse rigidity induced by normal forces, particular precautions must be taken in the global analysis, which is often delicate with conventional structural analysis codes. To do this, advanced computation software has to consider rest length state variables, geometric second-order terms in the rigidity matrix of elements, and slackening of cables. It also has to implement nonlinear schemes, such as Newton-Raphson (Quirant et al. 2003; Sanchez 2005). We can write the equilibrium as follows:

$$\mathbf{q}_0 = S\boldsymbol{\alpha} \quad (2)$$

The components of the vector $\boldsymbol{\alpha}$ are chosen to satisfy stress conditions for members.

Minigrid Self-Stress State

Tenségrité2000, local software developed by Quirant (2000), is able to determine the basic self-stress states of a tensegrity structure starting from the following:

- Boundary conditions: three nonsymmetrical support conditions here; and
- Geometry: node position and component connectivity.

Thus, the minigrid has only two basic self-stress states: a local self-stress state, SS1, and a diffuse self-stress state, SS2. Fig. 3 (thin lines for tensioned elements, thick lines for compressed ones) shows that for State SS1, peripheral elements are not involved in the equilibrium (white line), whereas for State SS2, this concerns only a few cables. By multiplying these basic states (vector values between -0.5 and 1 in this specific case) by the elements' free lengths l_i, the vectors of internal force $[Ti] = SSi \times l_i$ are obtained. The 2 vectors calculated [T1] and [T2] can be combined with two independent weighting coefficients a and b. Linear combination,
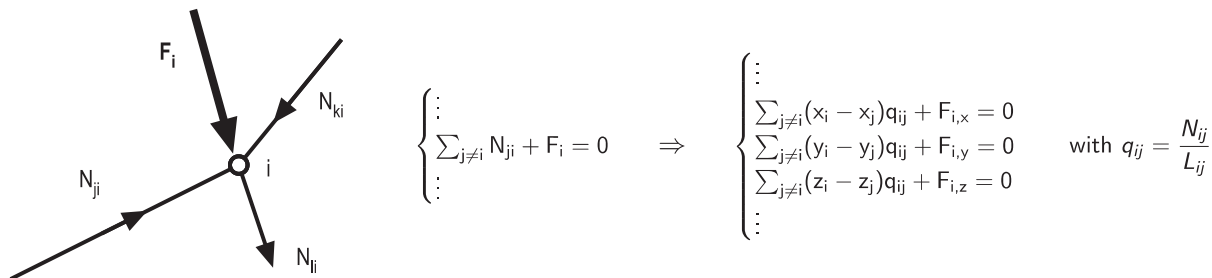

Fig. 2. Global static equilibrium

$a \times [T1] + b \times [T2]$, enables building a total self-stress state, which ensures the stability of the structure and the service limit states that is imposed.

By fixing ratio a/b, parameter a is used as an indicator of the self-stress level for the structure studied. The level is varied to obtain realistic values of the forces in each element to have a rather rigid structure without reaching the rupture point. A ratio of 0.5 gives the distribution of the forces in the components more homogeneity. Fig. 4 shows that the distribution of the tension in the cables is homogeneous. This result is important, because cables provide the structure with rigidity.

Identification of the Internal State

Standard Method

To identify self-stress state α_{id}, a method consistent with force measurements in a limited number of elements $\{T_{mes}\}$ selected to give independent information about both SS1 and SS2 and a single solution for identification was used. For that purpose, dedicated strain gauges were used (Fig. 5). The authors fit on the results of these measurements a state generated by the self-stress base (constituted by vector forces $[Ti]$ previously determined with a pseudoinverse method) to minimize the difference between the generated state and the measured state (Averseng 2004). This initial identification of the self-stress state, which is used as a reference, gives coefficients a and b, that is, a ratio a/b, near the target ratio (Fig. 5).

Minigrid Deformation under Static Loading

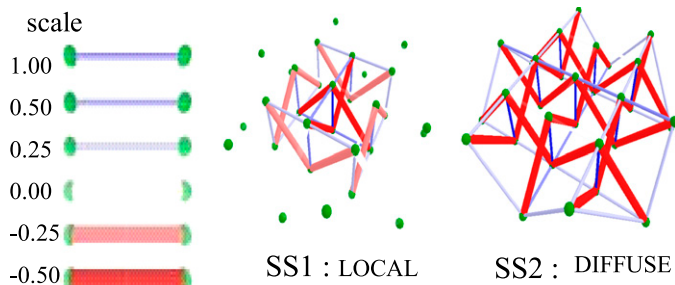To show the method of identifying of the self-stress level, the experimental deformation of the upper layer of the structure is used. To achieve this, a LEICA TDA5005 tachometer is used, combined with targets (reflectors CFR 1.5). Specific supports were manufactured to fix and center the target. Because the self-stress grid rigidity is high, forces great enough to obtain a measurable deformation of the grid must be applied. The authors opted for the successive application of loads to the six peripheral nodes in the lower layer that achieves an efficient total load (Fig. 6).

The measurements of the node displacement field are compared with the displacement field supplied by the simulation carried out by finite-element *Cast3M* version 2009 software (Verpeaux et al. 1988), in the case of several load series for a self-stress state close to a realistic state (Fig. 6). To calculate a lattice, the usual hypothesis
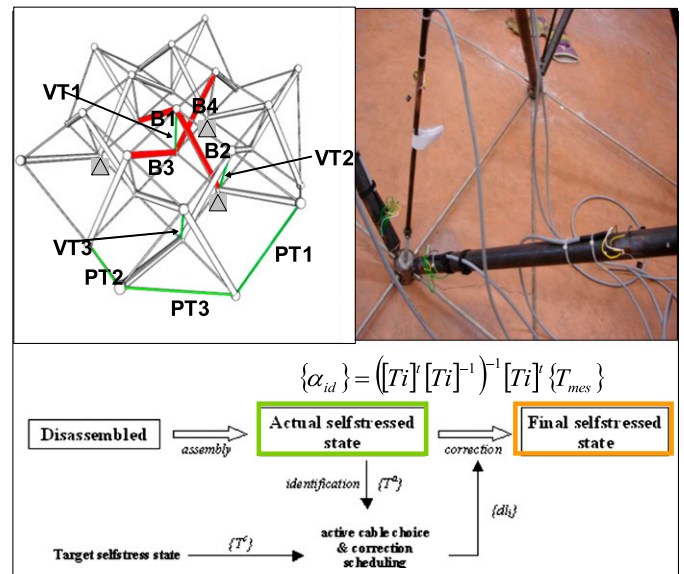
$$\{\alpha_{id}\} = \left([Ti]^t [Ti]^{-1}\right)^{-1} [Ti]^t \{T_{mes}\}$$

Fig. 5. Combination of tension vectors of the minigrid: experimental identification using force measurements

Fig. 3. Representation of the basic self-stress with a scale limited to 1
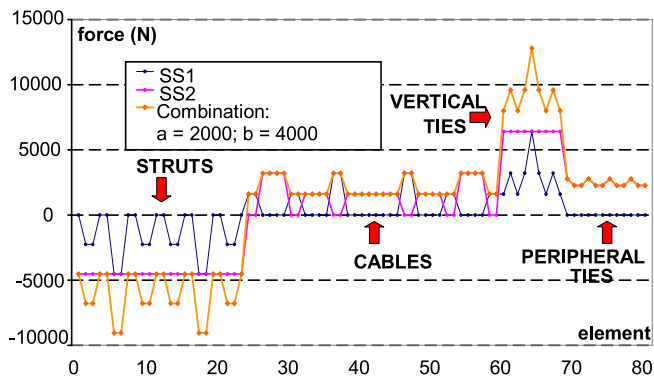
Fig. 4. Combination of force vectors of the minigrid for a realistic state

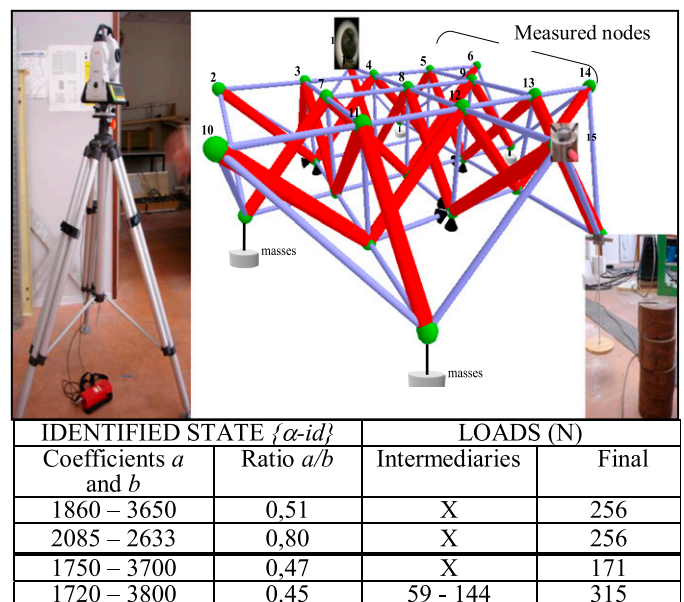| IDENTIFIED STATE {α-id}		LOADS (N)	
Coefficients a and b	Ratio a/b	Intermediaries	Final
1860 − 3650	0,51	X	256
2085 − 2633	0,80	X	256
1750 − 3700	0,47	X	171
1720 − 3800	0.45	59 - 144	315

Fig. 6. Load strategy in the minigrid's lower layer and measurement of displacement fields induced on the nodes of the upper layer (the tachometer, a reflector, its lodgings, and load application)

raised is a bar-type behavior for modeling all elements of a tensegrity structure. In our case, this assumption is affected by a previous study (Dubé et al. 2008), where the authors detected the bending in the struts with dedicated strain gauges. It was shown that, in static and dynamic loading, compressed elements and ties have a beam behavior. Only the cables can be modeled by bar elements (Fig. 6).

The first two attempts were carried out with the same 256-N loading for two different self-stress states, $a/b = 0.51$ and 0.80, leading to different force levels in elements. For the last two attempts, the authors focused on realistic states (a/b close to 0.5) to complete the load cases (171 and 315 N), including a loading with steps (59, 85, and 171 N). The vertical displacement, horizontal displacement and its direction (as an angle), and the force variation are compared during loading (Figs. 7 and 8). Qualitatively, a displacement field is found similar to the simulation. Fig. 7 shows the simulation of the node displacement for the upper layer according to the loading and measurements for some loads. The vertical displacements follow the load direction (Fig. 7, negative values of vertical displacement). It is different with Nodes 2, 13, 14, and 15 (positive values of vertical displacement) located behind the three Nodes (3, 9, and 12) with weak vertical displacements because of their connection to the support nodes through vertical ties. The maximum vertical displacements are observed for two peripheral nodes (10 and 14). Moreover, the load steps of the last experiment allow for visualization of the linear evolution of displacements.

Fig. 8 shows the evolution of horizontal displacements according to the loading for the top of the upper layer. A rotation

and a double shearing on the two sides of the line of nodes are distinguished passing through the central node, which almost does not move. Horizontal displacement maximums are obtained for peripheral nodes. The directions of displacements are in agreement with the experimental test and simulation.

Figs. 7 and 8 show that simulated displacements always underestimate the experimental ones. Table 1 gives absolute and relative values of these average differences of displacements and force variations. Classically, these differences can be attributed to the theoretical model, not taking into account the imperfections of links. But the authors can also refer to the fluctuations of forces in the elements identified by the measurements that show a difference between the actual self-stress state and the simulated state. There is a difference of less than 100 N between simulation and experimentation for forces of about 10 kN in the elements.

Relationship between Measurement of the Displacement Field Precision and Identification of the Self-Stress Level

The sensitivity was determined of the measurement of the displacement field versus the variation in the self-stress level around a design state: ratio a/b fixed to 0.5, with a varying in the interval 1,500–2,500 (Angellier et al. 2009). For this self-stress interval, the evolution of the average differences of vertical displacements obtained for several loads can be linearized (Fig. 9).
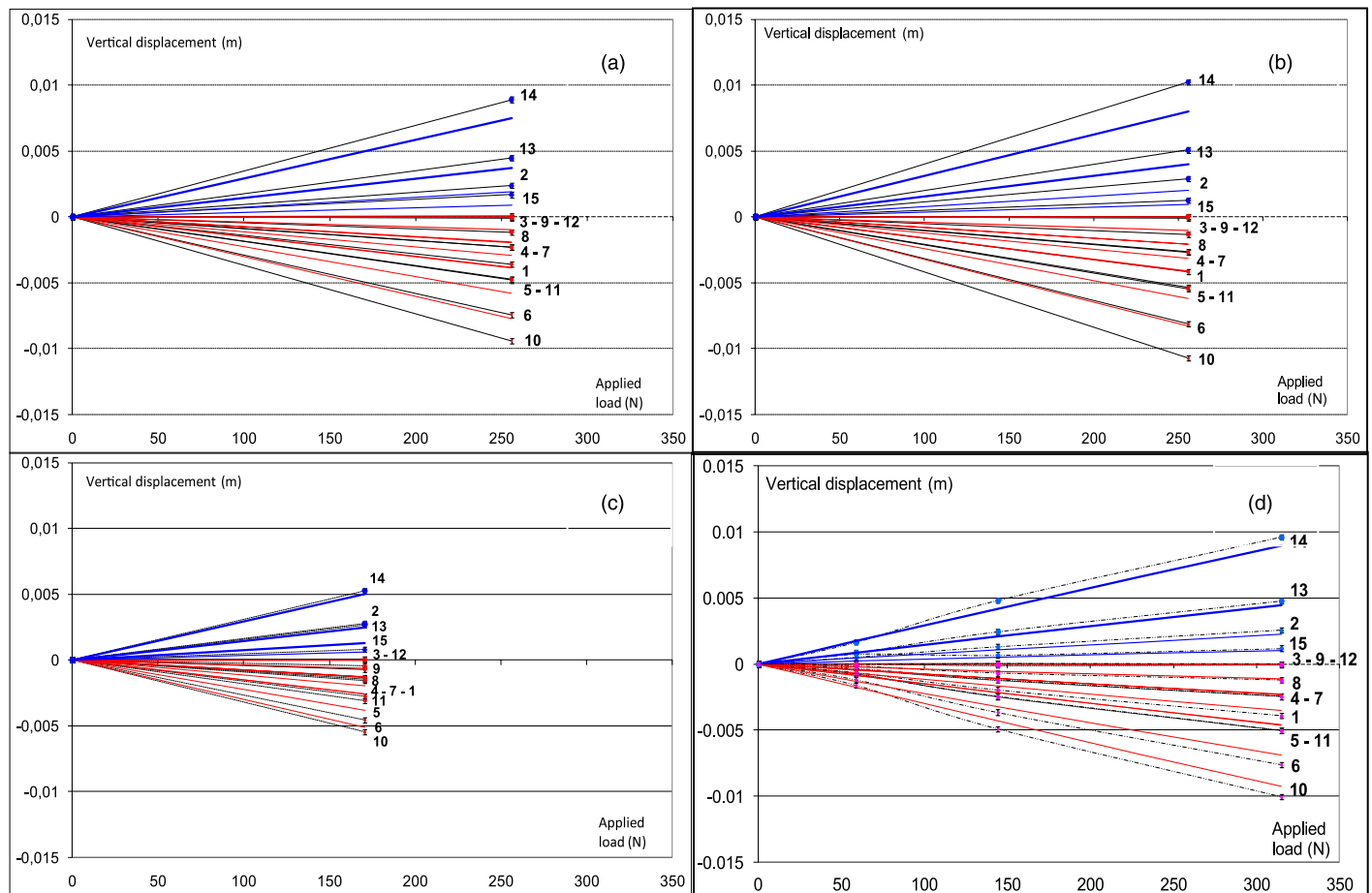

Fig. 7. Comparison between simulations (continuous lines) and measurements (dashes) for the vertical displacement of the upper layer: (a) load 256 N; (b) load 256 N; (c) load 171 N; (d) load 315 N
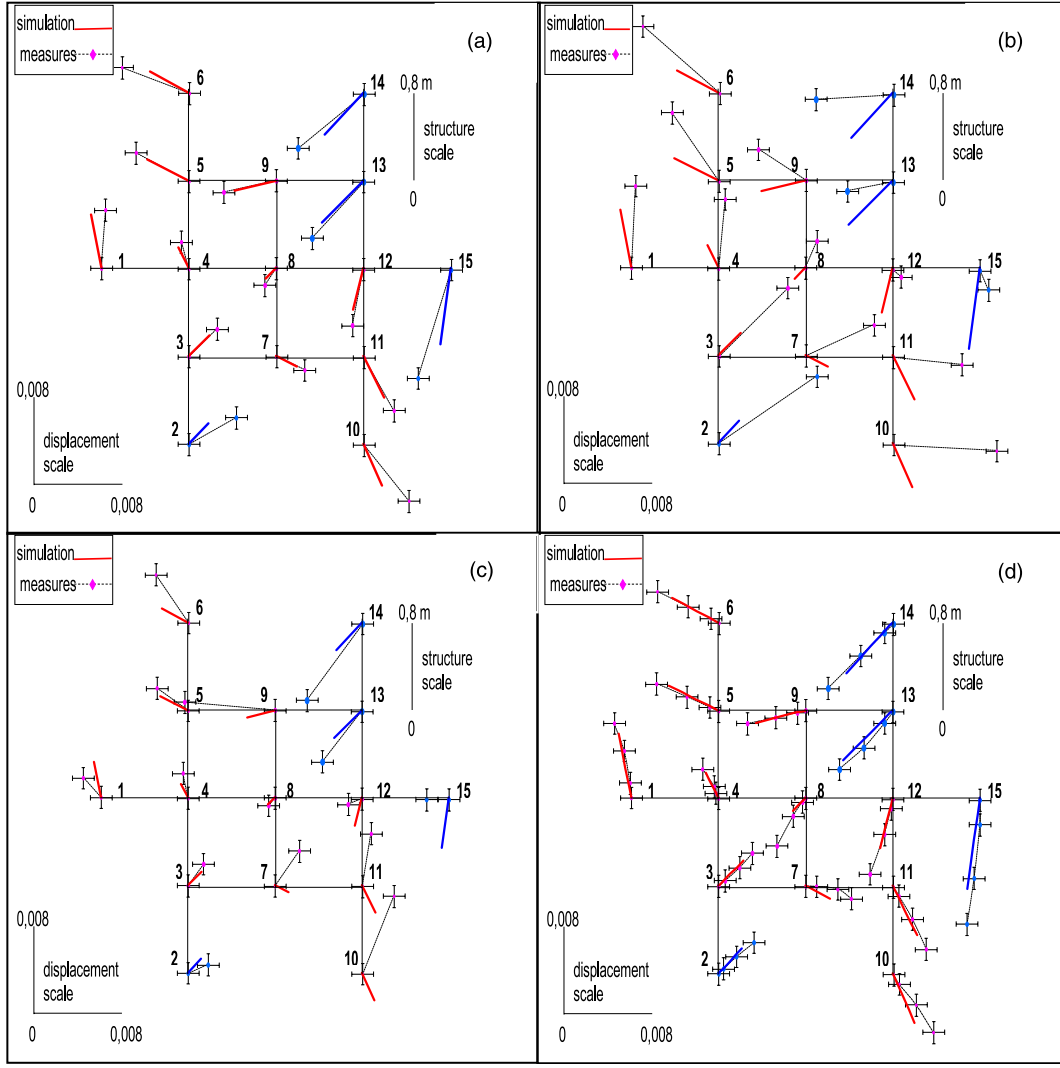
Fig. 8. Horizontal displacements of the upper layer (15 nodes): (a) load 256 N; (b) load 256 N; (c) load 171 N; (d) load 315 N

Table 1. Differences between Measurements and Simulations

Load step (N)	Average difference on vertical displacement (m)	Average difference on horizontal displacement (m)	Average difference on forces variations (N)
0–256	1.16×10^{-3} (24%)	3.42×10^{-3} (54%)	60 (28%)
0–256	8.90×10^{-4} (21%)	1.51×10^{-3} (29%)	60 (27%)
0–171	3.98×10^{-4} (17%)	2.16×10^{-3} (53%)	40 (27%)
0–315	3.80×10^{-4} (8%)	1.57×10^{-3} (26%)	80 (26%)

The slope value of this evolution allows for prediction of these average differences of displacements for any load

$$D_{V-1000}\left(10^{-4}m\right) = 0.022 \times F_6(N) \qquad (3)$$

where D_{V-1000} = vertical average differences of displacements for an a interval equal to 1000, and F_6 = load applied to the six peripheral nodes of the lower layer.

A strategy can be adopted by measuring the nodes that are most sensitive to the variation in self-stress: vertical displacement of Nodes 10 and 14. Fig. 9 enables us to find the following equation for a variation of a equal to 1,000:

$$D_{V-1000}\left(10^{-4}m\right) = 0.058 \times F_6(N) \qquad (4)$$

For Nodes 10 and 14, the ratio between the differences of displacement D and the differences between displacement fields measured and estimated allows for the identifiable interval of self-stress Δa to be determined. The precision of the self-stress level identification was determined with the experimental device for the minigrid. By using the most significant nodes, the authors suppose that the precision is greater.

The results are summarized in Table 2. The table shows the average differences of vertical displacements on the 15 nodes between experimental measurements and numerical simulations. The authors associate these results with the calculation of identifiable intervals Δa considering that the difference between measurement and simulation could be related to the precision of the experimental device.

In the first two load cases, a self-stress interval inferior to 1,000 with a vertical displacement is not identified; the third load case leads to good results. Indeed, for Steps 1 (0–59 N) and 3 (144–315 N), differences are obtained in vertical displacements in accordance with the estimated accuracy of the device. In Step 2 (59–144 N), differences higher than those found in Steps 1 and 3 are obtained. Concerning the global load, it is nonetheless possible to go below an interval of identifiable self-stress of 600. Moreover, despite a low load of 171 N, in Step 3, an interval of self-stress of 250 is identified,

that is, with a precision equivalent to the method using the direct measurements of forces, less than 15% error in the four experimental cases.

The results for the two sensitive nodes (Fig. 9) [Eq. (4)] are summarized in Table 3. As for the first load, an identifiable Δa is divided by more than 3, compared with the use of average measurements on the 15 nodes. The identification of the self-stress state is also equivalent to the method using the direct force measurements. Concerning the third load, the difference is 0.042 mm for Node 14. This leads to an identifiable Δa less than 50. By targeting these particular nodes, the error has been significantly reduced in the identification of the self-stress level compared with the use of the average of all nodes.

Conclusions

Good agreement was obtained between the digital simulations and experimental measurements. Experimental tests confirmed what the simulations results indicated: the structure subjected to vertical loading undergoes a general motion similar to a rotation, probably because of the asymmetry of boundary conditions and applied self-stress.

The following two strategies were shown to identify the self-stress level:
- The use of the average field of displacements gives good performances if experimental measurements are perfect; with imperfections the identification can lead to an erroneous result; and
- A correct identification is obtained of the self-stress ($<10\%$) starting from the nodes which move more and are most sensitive to the variations of the self-stress level.

With an important loading (up to 500 N) or a larger structure, the relative errors of measurement must have a lower influence. These results are promising enough to plan to identify the self-stress of the tensegrity grids in service starting from measurements of the displacement field. This procedure to determine the self-stress variation supposes to know the initial self-stress. To determine the initial self-stress, the authors can use classical method with local measurements. Within the framework of nondestructive control, the next stage is to carry out the same study with the vibratory response of the structure.
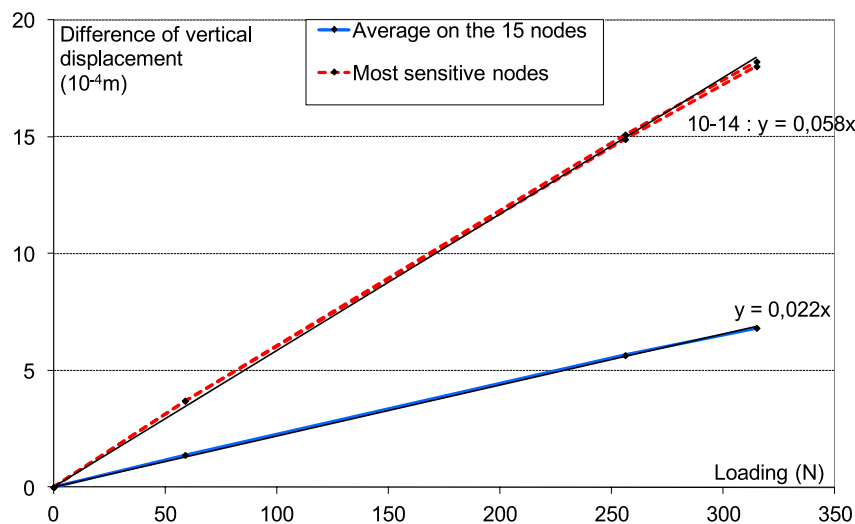

Fig. 9. Average differences of vertical displacements versus load with a coefficient variation equal to 1,000

Table 2. Maximum Differences between Simulation and Measurements of Vertical Displacements during a Static Loading—Determination of Identifiable Interval of Self-Stress Level

Load step (increment in N)	0–171 N (171)	Identified Δa	0–256 N (256)	Identified Δa				
Average difference on vertical displacement (m)	3.98×10^{-4}	1,100	8.90×10^{-4}	1,600			—	
Load step (increment in N)	Step 1: 0–59 N (59)	Identified Δa	Step 2: 59–144 N (85)	Identified Δa	Step 3: 144–315 N (171)	Identified Δa	Global: 0–315 N (315)	Identified Δa
Average difference on vertical displacement (m)	1.35×10^{-4}	1,100	3.99×10^{-4}	Errors of measures too large	9.26×10^{-5}	250	3.80×10^{-4}	600

Table 3. Maximum Differences between Simulation and Measurements for Sensitive Nodes—Determination of Identifiable Interval for Self-Stress Level

Load step (increment in N)		0–171 N (171)	Identified Δa	0–256 N (256)	Identified Δa	Step 3: 144–315 N (171)	Identified Δa
Average difference on vertical displacement (m)	Node 10	3.31×10^{-4}	340	1.79×10^{-3}	1,200	2.35×10^{-4}	240
	Node 14	2.67×10^{-4}	270	1.52×10^{-3}	1,030	4.20×10^{-5}	50

References

Angellier N., Dubé, J. F., Quirant J., Crosnier B. (2009). "Etude de la déformée d'une grille de tenségrité pour l'identification de son niveau d'autocontrainte." *Eur. J. Environ. Civil Eng.*, 13(10), 1183–1202 (in French).

Averseng, J. (2004). "Mise en œuvre et contrôle des systèmes de tenségrité." Ph.D. thesis, Université Montpellier 2, Montpellier, France (in French).

Averseng, J., and Crosnier, B. (2004a). "Prestressing tensegrity systems—Application to multiple selfstress systems." *Int. J. Struct. Stab. Dyn.*, 4(4), 543–557.

Averseng J., and Crosnier B. (2004b). "Static and dynamic robust control of tensegrity systems." *J. Int. Assoc. Shell Spat. Struct.*, 45(3), 169–174.

Barcilon, V. (1982). " Inverse mode problems for the vibrating beam in the free-clamped configuration." *Philosoph. Trans. Royal Soc. London A: Math. Phys. Trans.*, 304(1483), 211–251.

Bicanic, N., and Chen, H. P. (1997). "Damage identification in framed structures using natural frequencies." *Int. J. Numer. Methods Eng.*, 40(23), 4451–4468.

Dubé, J. F. (2004). "Identification de l'endommagement d'une poutre par analyse vibratoire." *Revue Française de Génie-Civil*, 8(2–3), 203–218 (in French).

Dubé, J. F., Angellier, N., and Crosnier, B. (2008). "Comparison between experimental tests and numerical simulations carried out on a tensegrity minigrid." *Eng. Struct.*, 30(7), 1905–1912.

Fuller, R. B. (1973). *The dymaxion world of Buckminster Fuller*, Anchor, New York.

Gurdal, Z., Haftka, R. T., and Kamat, M. P. (1993). *Elements of structural optimization*, Kluwer, Dordrecht, Netherlands.

Kawaguchi, K., and Lu, Z. Y. (2002). " Construction of three-strut tension systems." *Space Structures 5,* T. Telford, G. Parke, and P. Disney, eds., Guilford, U.K., 1, 1–10.

Maeck, J., et al. (2000). "Damage identification in reinforced concrete structures by dynamic stiffness determination." *Eng. Struct.*, 22(10), 1339–1349.

Motro, R. (2002). "Tensarch project." *Space Structures 5*, T. Telford, G. Parke, and P. Disney, eds., Guilford, U.K., 1, 57–66.

Motro, R. (2003). *Tensegrity: Structural systems for the future*, Kogan Page Science, London.

Murakami, H., and Nishimura, Y. (2001). "Static and dynamic characterization of some tensegrity modules." *J. Appl. Mech.*, 68(1), 19–27.

Ndambi, J. M., et al. (2000). "Comparison of techniques for modal analysis of concrete structures." *Eng. Struct.*, 22(9), 1159–1166.

Oda, K., and Hangai, Y. (1995). "Optimal self-equilibrated stresses in cables structures." *Spatial structures: Heritage, present and future*, Proc., Int. Assoc. of Space Struct. Symp., G. C. Giuliani, ed., S. G. Editoriali, Padova, Italy, 859–864.

Olhof, N., Eschenauer, H., and Schnell, W. (1997). *Applied structural mechanics. Structural optimization*, Springer, Berlin, Germany.

Pritchard, J. I., Adelman, H. M., and Haftka, R. T. (1987). "Sensitivity analysis and optimization of nodal point placement for vibration reduction." *J. Sound Vibrat.*, 119(2), 277–289.

Quirant, J. (2000). "Systèmes de tenségrité et autocontrainte: Qualification, sensibilité et incidence sur le comportement." Ph.D. thesis, Université Montpellier 2, Montpellier, France (in French).

Quirant, J., Kazi Aoual, M. N., and Laporte, R. (2003). "Tensegrity systems: The application of linear programming in search of compatible self-stress states." *J. Int. Assoc. Shell Spat. Struct.*, 44(1), 33–50.

Sanchez, L. R. (2005). "Contribution à l'étude mécanique des systèmes de tenségrité." Ph.D. thesis, Université Montpellier 2, Montpellier, France (in French).

Snelson, K. (1973). *Tensegrity mast*, Shelter, Bolinas, CA.

Van Den Abeele, K., and DeVisscher, J. (2000). "Damage assessment in reinforced concrete using spectral and temporal nonlinear vibration techniques." *Cement Concr. Res.*, 30(9), 1453–1464.

Verpeaux, P., Charras, T., and Millard, A. (1988). "Castem2000, une approche moderne du calcul des structures." *Calcul des structures et intelligence artificielle*, J. M. Fouet, P. Ladevèze, and R. Ohayon, eds., Pluralis, France, 2, 261–271.